Reflection-mode photoacoustic microscopy using a hollow focused ultrasound transducer for *in vivo* imaging of blood vessels*

Yuan Yi(袁 毅) and Yang Si-Hua(杨思华)†

MOE Key Laboratory of Laser Life Science & Institute of Laser Life Science, College of Biophotonics, South China Normal University, Guangzhou 510631, *China*

(Received 22 October 2011; revised manuscript received 19 December 2011)

A reflection-mode photoacoustic microscope using a hollow focused ultrasound transducer is developed for high-resolution *in vivo* imaging. A confocal structure of the laser and the ultrasound is used to improve the system resolution. The axial and lateral resolutions of the system are measured to be $\sim$ 32 μm and $\sim$ 58 μm, respectively. *Ex vivo* and *in vivo* modes are tested to validate the imaging capability of the photoacoustic microscope. The adjacent vein and artery can be seen clearly from the reconstructed photoacoustic images. The results demonstrate that the reflection-mode photoacoustic microscope can be used for high-resolution imaging of micro-blood vessels, which would be of great benefit for monitoring the neovascularization in tumor angiogenesis.

Keywords: photoacoustic microscopy, hollow focused ultrasound transducer, blood vessels

PACS: 42.62.–b **DOI:** 10.1088/1674-1056/21/5/054211

1. Introduction

Photoacoustic (PA) imaging is based on the generation of acoustic waves when a pulsed laser is absorbed by tissue chromophores. A thermoelastic pressure transient is generated by the induced temperature rise. The amplitude of the generated ultrasound is dependent on the amount of the absorbed light that is determined by the local energy fluence and the optical absorption coefficient of the target tissue. As a high-resolution, high-contrast, and noninvasive imaging modality,[1−6] PA imaging has recently attracted considerable attention and been suggested as a new technique for noninvasive imaging of blood vessels.[7−13] Compared to optical imaging technology,[14−15] PA imaging has a better penetration depth.

In this study, a reflection-mode PA microscope using a hollow focused ultrasound transducer is developed for imaging blood vessels. It has a confocal structure for the light and the ultrasound. The axial and lateral resolutions of the system are quantitatively analyzed to be $\sim$ 32 μm and $\sim$ 58 μm, respectively. The PA images of the simulation sample and the *ex vivo* blood vessels of a mouse's back are reconstructed by using the maximum amplitude projection algorithm.[16] Furthermore, experiments of imaging the *in vivo* blood vessels of a mouse's back are performed with the system. The results demonstrate that the system can reconstruct PA images of biological tissue *in vivo* with high contrast and high resolution. It could be used for monitoring the neovascularization in tumor angiogenesis.

2. Imagining system

2.1. Imaging principle

The schematic diagram and the coordinates of the hollow focused ultrasound transducer are shown in Fig. 1. In theory, according to the Rayleigh integral, the sound field distribution function of the hollow focused ultrasound transducer can be expressed as

$$p = \mathrm{j}kc\rho \iint_S \frac{u}{2\pi r_1} \mathrm{e}^{-\mathrm{j}kr_1} \mathrm{e}^{-\alpha r_1} \mathrm{d}S, \qquad (1)$$

where k is the wave number, c is the speed of sound, ρ is the mass density, u is the surface velocity, α is the

*Project supported by the National Basic Research Program of China (Grant Nos. 2010CB732602 and 2011CB910402), the Program for Changjiang Scholars and Innovative Research Team in University, China (Grant No. IRT0829), the National Natural Science Foundation of China (Grant Nos. 30870676, 81127004 and 11104087), and the Foundation for Distinguished Young Talents in Higher Education of Guangdong, China (Grant No. LYM10061).

†Corresponding author. E-mail: yangsh@scnu.edu.cn

© 2012 Chinese Physical Society and IOP Publishing Ltd

attenuation coefficient of the medium, and r_1 is the distance between integral element $\mathrm{d}S$ and space point Q. The integral element $\mathrm{d}S$ can be expressed as

$$\mathrm{d}S = R_1 \,\mathrm{d}R_1 \,\mathrm{d}\beta, \tag{2}$$

where β is the azimuth difference between integral element $\mathrm{d}S$ and space point Q, R_1 is the distance between the origin of the coordinate and integral element $\mathrm{d}S$. The r_1 can be given by

$$r_1 = \left[r_0^2 - 2r_0 R_1 \sqrt{1 - \frac{R_1^2}{4R^2}} \sin\theta\cos\beta + R_1^2 \left(1 - \frac{r_0 \cos\theta}{R}\right)\right]^{1/2}, \tag{3}$$

where r_0 is the distance between space point Q and the origin of the coordinate, θ is the angle between r_0 and the z axis and can be expressed as

$$\theta = \arctan\left(\frac{r_0}{z}\right). \tag{4}$$

Combining formulae (1)–(4), on the focal plane of $z = R$, we can express the length of the ultrasonic focal spot along the z axis as

$$\Delta z = 4\frac{\lambda R^2}{b^2}, \tag{5}$$

where λ is the wavelength of the acoustic wave, b is the distance between the z axis and the edge of the transducer. The radius of the ultrasonic focal spot perpendicular to the z axis can be expressed as

$$\Delta r = 0.61\frac{\lambda R}{b}. \tag{6}$$

The distance between the ultrasonic focal spot and the transducer bottom is 9 mm. Radius b and distance R are 10 mm and 13.45 mm, respectively. The hollow focused ultrasound transducer has a center frequency of 15 MHz, the corresponding wavelength λ is 10^{-4} m. According to formulae (5) and (6), the length and the radius of the ultrasonic focal spot are 723.6 μm and 82.05 μm, respectively.

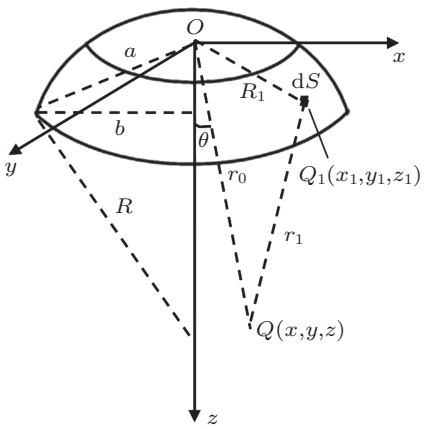


Fig. 1. Schematic diagram and coordinates of the hollow focused ultrasound transducer. The length and the radius of the ultrasonic focal spot can be calculated by using the parameters in the diagram.

2.2. Experimental system

The schematic diagram of the experimental setup is shown in Fig. 2(a). An Nd:YAG laser, operating at a wavelength of 532 nm with a full width at half maximum (FWHW) of 10 ns and a repetition of 15 Hz, was used in the experiment as the light source. Light reflected by a reflector was focused by a condenser lens. The focusing light passed through a pinhole, and then was focused by another condenser lens. A hollow focused ultrasound transducer was used to receive the PA signals from the test sample. Figure 2(b) is a photograph of the hollow focused ultrasound transducer with a length of 65 mm. Its inner and outer diameters were 2.7 mm and 20 mm, respectively. The test sample was fixed onto a sample support under a water container. The water container was filled with water, which was used as the ultrasonic coupling medium. The test sample and the ultrasonic coupling medium were separated by a transparent plastic film to prevent them from contacting each other. The light and the ultrasound were confocal in the experimental setup. The focusing light, which passed through the hollow focused ultrasound transducer and the ultrasonic coupling medium, irradiated the sample surface to generate the PA signals.

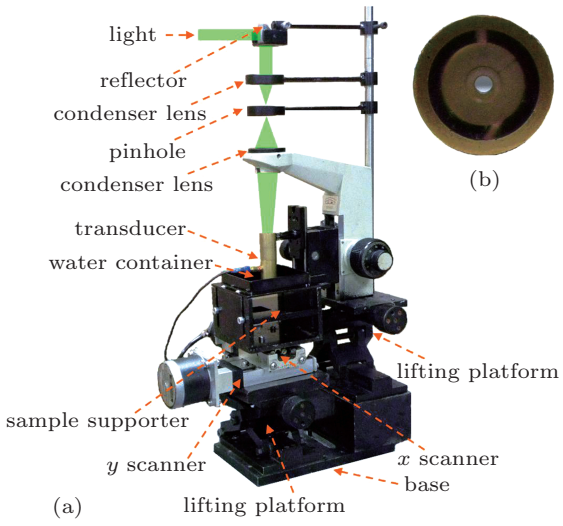


Fig. 2. (colour online) (a) Schematic diagram of the experimental setup, (b) photograph of the hollow focused ultrasound transducer.

The sample support was mounted in an x–y scanning system to scan over the test sample. The x–y scanning system was controlled by a computer and triggered by the trigger signals of the pump laser. The PA signals generated by the test sample were recorded by a computer through an amplifier and a dual-channel data acquisition card, the sampling rate of the data acquisition card was 100 M/s.

3. Results

3.1. Resolution of the imaging system

To evaluate the imaging capability of the PA microscope system, a human hair with a diameter of $\sim$ 55 μm was imaged. The hair was placed in the confocal region of the light and the ultrasound. Figure 3(a) shows the reconstructed PA cross-section image of the hair, whereas Fig. 3(b) shows the PA signals at the locations marked by the red dotted line in Fig. 3(a). The axial resolution is estimated to be 32 μm from Fig. 3(b).[17] Figure 3(c) is the reconstructed profile of the region marked by the red dotted line in Fig. 3(a). The lateral resolution is estimated to be 58 μm from Fig. 3(b).[17] If the tested sample is not located in the confocal region, the lateral resolution will be worse.

3.2. PA imaging of simulation sample and *ex vivo* blood vessels of a mouse's back

To demonstrate the imaging ability of the PA microscopy system, a simulation sample and *ex vivo* blood vessels of a mouse's back were used in the experiment. The simulation sample consisted of three human hairs with diameters of $\sim$ 50 μm, $\sim$ 55 μm, and $\sim$ 40 μm, respectively. The sample was immersed in a transparent phantom with a depth of $\sim$ 1 mm. The phantom was made of 8% gelatin and 92% water. Figure 4(a) is the reconstructed PA cross-section image of these human hairs. The corresponding photograph of the three hairs is shown in the insert of Fig. 4(a). We can see that the PA image with good contrast and high resolution is in good agreement with the sample. Figure 4(b) is the reconstructed profile of the region marked by the red dotted line in Fig. 4(a). It shows the different diameters of the hairs.

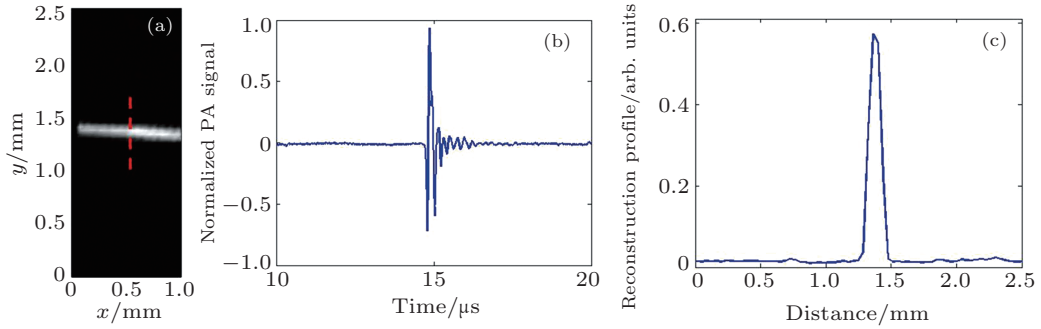


Fig. 3. (colour online) (a) PA cross-section image of a human hair with a diameter of 55 μm, (b) corresponding PA signals at the locations marked by the red dotted line, (c) reconstructed profile of the region marked by the red dotted line.

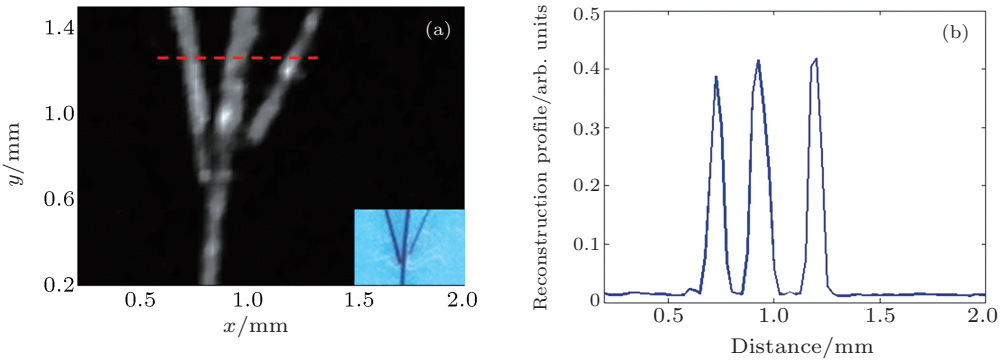


Fig. 4. (colour online) (a) PA cross-section image of three human hairs, (b) reconstructed profile of the region marked by the red dotted line. The insert is the photograph of the hairs.

In the next experiment, a BALB/c mouse with a body weight of 30 g was used for imaging *ex vivo* blood vessels of a mouse's back. The fur on the mouse's back was shaven and chemically depilated before imaging. The mouse was anesthetized until death, and its back skin along with blood vessels was removed. The skin was cleaned with a 0.9% sodium chloride irrigation solution and embedded in a transparent gelatin phantom. Figure 5(a) is a photograph of the *ex vivo* blood vessels of the mouse's back. The reconstructed PA image of the blood vessels is shown in Fig. 5(b). A satisfactory match between the photograph and the reconstructed image can be seen at the positions marked with A, B, C, D.

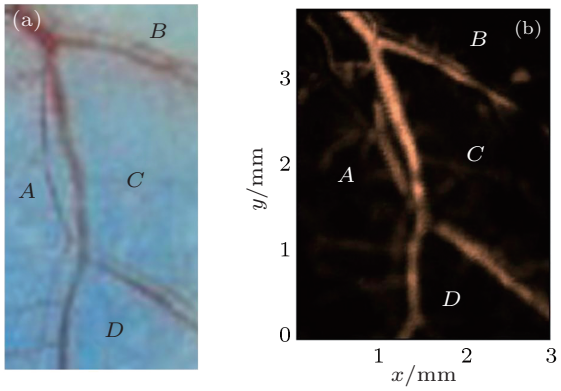


Fig. 5. (colour online) (a) Photograph of the *ex vivo* blood vessels of the mouse's back, (b) reconstructed PA image of the *ex vivo* blood vessels of the mouse's back.

Nonuniform contrast is shown in the PA image of the blood vessels, which is probably caused by the uneven distribution of blood in the *ex vivo* blood vessels. These experimental results verify that the PA microscopy system is capable of imaging samples with high contrast and high resolution.

3.3. PA imaging of the blood vessels of a mouse's back *in vivo*

The PA microscopy system can also *in vivo* image the blood vessels. A BALB/c mouse with a body weight of 25 g was used for the experiments. The fur on the mouse's back was shaven and chemically depilated before imaging. General anesthesia (i.e., sodium pentobarbital, 40 mg/kg; supplemental, 10 mg/kg/h or as necessary) was applied to keep the mouse static during the experiment. Figure 6(a) is a photograph of the mouse, and the imaging region is marked by a red dashed rectangle box. Figure 6(b) is the reconstructed PA image of the *in vivo* blood vessels of the mouse's back. In Fig. 6(b), the structure of the blood vessels can be seen clearly. One of the blood vessels in Fig. 6(b) is indicated by an arrow, the diameter of the microvascular vessel is ~ 62 μm. The experimental result shows that the PA microscopy system is able to image the blood vessels *in vivo*.

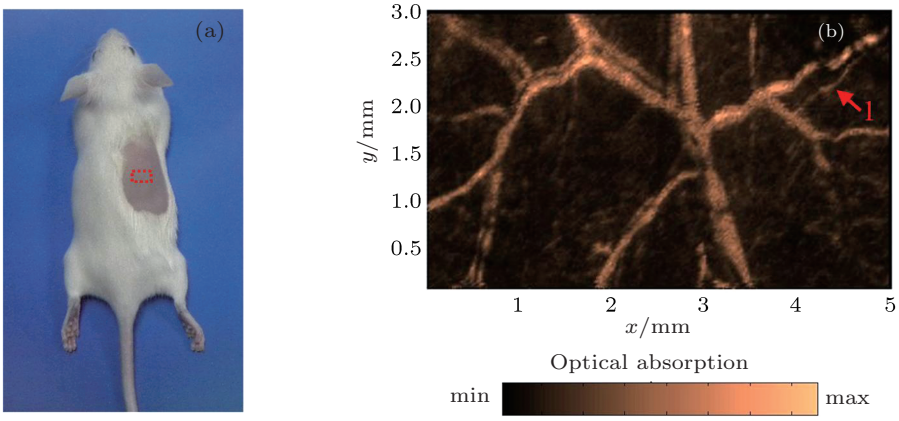


Fig. 6. (colour online) (a) *in vivo* photograph of the mouse, (b) reconstructed PA image of the *in vivo* blood vessels of the mouse's back marked by the red dashed rectangular box.

4. Discussion and conclusion

The experimental results show that PA images of biological tissues can be reconstructed with high contrast and high resolution by using the PA microscopy system. However, the resolution of the system is insufficient to image the microvascular vessels with a diameter less than 50 μm. In our next work, a microscope objective will be used to focus the pulsed laser and the length of the hollow focused ultrasound transducer will be decreased, so that the light can be focused in the test sample. The rate of the data acquisition is controlled by the repetition rate of the pulsed laser. Due to the limitations of the laser repetition

rate, real-time dynamic imaging and monitoring could not be achieved in the present study. Real-time dynamic imaging and monitoring could be achieved by using a laser with a repetition frequency of 24 Hz or higher in the future.

In summary, we developed a reflection-mode PA microscope using a hollow focused ultrasound transducer. The simulation sample and *ex vivo* blood vessels were imaged. Furthermore, the image of blood vessels in a mouse back was *in vivo* reconstructed by using the system. The results demonstrated that reflection-mode PA microscope had the ability to image biological tissues. PA vascular imaging is an important application of PA imaging technology, which can be used to detect and monitor vascular tumor proliferation and blood oxygenation. The system has potential applications for monitoring the neovascularization in tumor angiogenesis.

References

[1] Yin B Z, Xing D, Wang Y, Zeng Y G, Tan Y and Chen Q 2004 *Phys. Med. Biol.* **49** 1339

[2] Wang Y, Xing D, Zeng Y G and Chen Q 2004 *Phys. Med. Biol.* **49** 3117

[3] Wang X D, Pang Y J, Ku G, Xie X Y, Stoica G and Wang L V 2003 *Nat. Biotechnol.* **21** 803

[4] Xiang L Z, Xing D, Gu H M, Yang D W, Yang S H and Zeng L M 2007 *Acta Phys. Sin.* **56** 3911 (in Chinese)

[5] Zeng Y G, Xing D, Wang Y, Yin B Z and Chen Q 2004 *Opt. Lett.* **2** 1760

[6] Kruger R A, Liu P Y, Fang Y R and Appledorn C R 1995 *Med. Phys.* **22** 1605

[7] Yang S H, Xing D, Zhou Q, Xiang L Z and Lao Y Q 2007 *Med. Phys.* **34** 3294

[8] Zhang H F, Maslov K, Li M L, Stoica G and Wang L V 2006 *Opt. Express* **14** 9317

[9] Yang S H and Yin G Z 2009 *Acta Phys. Sin.* **58** 4760 (in Chinese)

[10] Yang S H, Xing D, Lao Y Q, Yang D W, Zeng L M, Xiang L Z and Chen W R 2007 *Appl. Phys. Lett.* **90** 243902

[11] Xiang L Z, Xing D, Guo H, Yang S H and Yang D W 2009 *Acta Phys. Sin.* **58** 238 (in Chinese)

[12] Wang H, Xing D and Xiang L Z 2008 *J. Phys.* D: *Appl. Phys.* **41** 095111

[13] Yang D W, Xing D, Gu H M, Tan Y and Zeng L M 2005 *Appl. Phys. Lett.* **87** 194101

[14] Wang K, Zeng Y, Ding Z H, Meng J, Shi G H and Zhang Y D 2010 *Acta Phys. Sin.* **59** 2471 (in Chinese)

[15] Lu J, Li H, He Y, Shi G H and Zhang Y D 2011 *Acta Phys. Sin.* **60** 266 (in Chinese)

[16] Maslov K, Stoica G and Wang L H 2005 *Opt. Lett.* **30** 625

[17] Cui H Z and Yang X M 2010 *Med. Phys.* **37** 4777